Nonnegative autoencoder with simplified random neural network

Yonghua Yin, Erol Gelenbe
Intelligent Systems and Networks Group, Electrical & Electronic Engineering Department
Imperial College, London SW7 2AZ, UK
`y.yin14@imperial.ac.uk, e.gelenbe@imperial.ac.uk`

Abstract

This paper proposes new nonnegative (shallow and multi-layer) autoencoders by combining the spiking Random Neural Network (RNN) model, the network architecture typical used in deep-learning area and the training technique inspired from nonnegative matrix factorization (NMF). The shallow autoencoder is a simplified RNN model, which is then stacked into a multi-layer architecture. The learning algorithm is based on the weight update rules in NMF, subject to the nonnegative probability constraints of the RNN. The autoencoders equipped with this learning algorithm are tested on typical image datasets including the MNIST, Yale face and CIFAR-10 datasets, and also using 16 real-world datasets from different areas. The results obtained through these tests yield the desired high learning and recognition accuracy. Also, numerical simulations of the stochastic spiking behavior of this RNN auto encoder, show that it can be implemented in a highly-distributed manner.

1   Introduction

A mathematical tool that has existed since 1989 [1–3], but is less well known in the machine-learning community, is the Random Neural Network (RNN), which is a stochastic integer-state "integrate and fire" system and developed to mimic the behaviour of biological neurons in the brain. In an RNN, an arbitrarily large set of neurons interact with each other via excitatory and inhibitory spikes which modify each neuron's action potential in continuous time. The power of the RNN lays on the fact that, in steady state, the stochastic spiking behaviors of the network have a remarkable property called "product form" and that the state probability distribution is given by an easily solvable system of non-linear equations. The RNN has been used for numerous applications [4–15] that exploit its recurrent structure.

Deep learning has achieved great success in machine learning [16,17]. Many computational models in deep learning exploit a feed-forward neural-network architecture that is composed of multi-processing layers, which allows the model to extract high-level representations from raw data. The feed-forward fully-connected multi-layer neural network could be difficult to train [18]. Pre-training the network layer by layer is a great advance [16, 19] and useful due to its wide adaptability, though recent literature shows that utilizing the rectified linear unit (ReLU) could train a deep neural network without pre-training [20]. The typical training procedure called stochastic gradient descent (SGD) provides a practical choice for handling large datasets [21].

Nonnegative matrix factorization (NMF) is also a popular topic in machine learning [22–26], which learns part-based representations of raw data. Lee [22] suggested that the perception of the whole in the brain may be based on these part-based representations (based on the physiological evidence [27]) and proposed simple yet effective update rules. Hoyer [24] combined sparse coding and NMF that allows control over sparseness. Ding investigated the equivalence between the NMF and K-means

clustering in [26, 28] and presented simple update rules for orthogonal NMF. Wang [25] provided a comprehensive review on recent processes in the NMF area.

This paper first exploits the structure of the RNN equations as a quasi-linear structure. Using it in the feed-forward case, an RNN-based shallow nonnegative autoencoder is constructed. Then, this shallow autoencoder is stacked into a multi-layer feed-forward autoencoder following the network architecture in the deep learning area [16, 17, 19]. Since connecting weights in the RNN are products of firing rates and transition probabilities, they are subject to the constraints of nonnegativity and that the sum of probabilities is no larger than 1, which are called the RNN constraints in this paper. In view of that, the conventional gradient descent is not applicable for training such an autoencoder. By adapting the update rules from nonnegative graph embedding that can be seemed as a variant of NMF, applicable update rules are developed for the autoencoder that satisfy the first RNN constraint of nonnegativity. For the second RNN constraint, we impose a check-and-adjust procedure into the iterative learning process of the learning algorithms. The training procedure of SGD is also adapted into the algorithms. The efficacy of the nonnegative autoencoders equipped with the learning algorithms is well verified via numerical experiments on both typical image datasets including the MNIST [29], Yale face [30] and CIFAR-10 [31] datesets and 16 real-world datasets in different areas from the UCI machine learning repository [32]. Then, we simulate the spiking behaviors of the RNN-based autoencoder, where simulation results conform well with the corresponding numerical results, therefore demonstrating that this nonnegative autoencoder can be implemented in a highly-distributed and parallel manner.

2 A quasi-linear simplified random neural network

An arbitrary neuron in the RNN can receive excitatory or inhibitory spikes from external sources, in which case they arrive according to independent Poisson processes. Excitatory or inhibitory spikes can also arrive from other neurons to a given neuron, in which case they arrive when the sending neuron fires, which happens only if that neuron's input state is positive (i.e. the neuron is excited) and inter-firing intervals from the same neuron v are exponentially distributed random variables with rate $r_v \geq 0$. Since the firing times depend on the internal state of the sensing neuron, the arrival process of neurons from other cells is not in general Poisson. From the preceding assumptions it was proved in [3] that for an arbitrary N neuron RNN, which may or may not be recurrent (i.e. containing feedback loops), the probability in steady-state that any cell h, located anywhere in the network, is excited is given by the expression:

$$q_h = \min\left(\frac{\lambda_h^+ + \sum_{v=1}^N q_v r_v p_{vh}^+}{r_h + \lambda_h^- + \sum_{v=1}^N q_v r_v p_{vh}^-}, 1\right), \tag{1}$$

for $h = 1, \ldots, N$, where p_{vh}^+, p_{vh}^- are the probabilities that cell v may send excitatory or inhibitory spikes to cell h, and λ_h^+, λ_h^- are the external arrival rates of excitatory and inhibitory spikes to neuron h. Note that $\min(a, b)$ is a element-wise operation whose output is the smaller one between a and b. In [3], it was shown that the system of N non-linear equations (1) have a solution which is unique.

Before adapting the RNN as a non-negative autoencoder (Section 3), we will simplify the recurrent RNN model into the feed-forward structure shown in Figure 1. The simplified RNN has an input layer and a hidden layer. The V input neurons receive excitatory spikes from the outside world, and they fire excitatory spikes to the H hidden neurons.

Let us denote by $\hat{q}_v$ the probability that the vth input neuron ($v = 1, \cdots, V$) is excited and q_h the probability that the hth hidden neuron ($h = 1, \cdots, H$) is excited. According to [1] and (1), they are given by $\hat{q}_v = \min(\hat{\Lambda}_v^+/\hat{r}_v, 1)$, and $q_h = \min(\Lambda_h^+/r_h, 1)$, where the quantities $\hat{\Lambda}_v^+$ and Λ_h^+ represent the total average arrival rates of excitatory spikes, $\hat{r}_v$ and r_h represent the firing rates of the neurons. Neurons in this model interact with each other in the following manner, where $h = 1, \cdots, H$ and $v = 1, \cdots, V$. When the vth input neuron fires, it sends excitatory spikes to the hth hidden neuron with probability $p_{v,h}^+ \geq 0$. Clearly, $\sum_{h=1}^H p_{v,h}^+ \leq 1$.
• The vth input neuron receives excitatory spikes from the outside world with rate $x_v \geq 0$.
• When the hth hidden neuron fires, it sends excitatory spikes outside the network.

Let us denote $w_{v,h} = p_{v,h}^+ \hat{r}_v$. For simplicity, let us set the firing rates of all neurons to $\hat{r}_v = r_h = 1$ or that $\sum_{h=1}^H w_{v,h} \leq 1$. Then, $\hat{\Lambda}_v^+ = x_v$, $\hat{r}_v = 1$, $\Lambda_h^+ = \sum_{v=1}^V w_{v,h}\hat{q}_v$, and using the fact that q_h, q_v
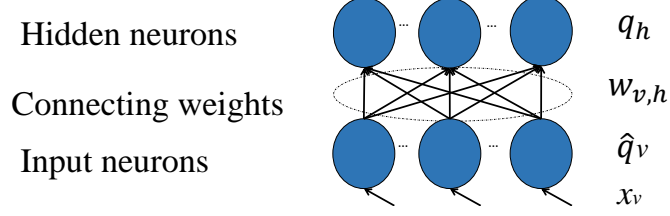
Figure 1: Brief model structure of the quasi-linear RNN.

are probabilities, we can write:

$$\hat{q}_v = \min(x_v, 1), \ q_h = \min(\sum_{v=1}^{V} w_{v,h}\hat{q}_v, 1), \tag{2}$$

subject to $\sum_{h=1}^{H} w_{v,h} \leq 1$. We can see from (2) that this simplified RNN is quasi linear. For the network shown in Figure 1, we call it a quasi-linear RNN (LRNN).

3 Shallow non-negative LRNN autoencoder

We add an output layer with O neurons on top of the hidden layer of the LRNN shown in Figure 1 to construct a shallow non-negative LRNN autoencoder. Let $\overline{q}_o$ denote the probability that the oth output neuron is excited, and the oth output neurons interact with the LRNN in the following manner, where $o = 1, \cdots, O$.
• When the hth hidden neuron fires, it sends excitatory spikes to the oth output neuron with probability $\overline{p}_{h,o}^+ \geq 0$. Also, $\sum_{o=1}^{O} \overline{p}_{h,o}^+ \leq 1$.
• The firing rate of the oth output neuron $\overline{r}_o = 1$.
Let $\overline{w}_{h,o} = \overline{p}_{h,o}^+ r_h = \overline{p}_{h,o}^+$. Then, $\sum_{o=1}^{O} \overline{w}_{h,o} \leq 1$. The shallow LRNN autoencoder is described by

$$\hat{q}_v = \min(x_v, 1), \ q_h = \min(\sum_{v=1}^{V} w_{v,h}\hat{q}_v, 1), \ \overline{q}_o = \min(\sum_{h=1}^{H} \overline{w}_{h,o}q_h, 1), \tag{3}$$

where $O = V$ and the input, hidden and output layers are the visual, encoding and decoding layers.

Suppose there is a dataset represented by a nonnegative $D \times V$ matrix $X = [x_{d,v}]$, where D is the number of instances, each instance has V attributes and $x_{d,v}$ is the vth attribute of the dth instance. We import X into the input layer of the LRNN autoencoder. Let $\hat{q}_{d,v}$, $q_{d,h}$ and $\overline{q}_{d,o}$ respectively denote the values of $\hat{q}_v$, q_d and $\overline{q}_o$ for the dth instance.

Let a $D \times V$-matrix $\hat{Q} = [\hat{q}_{d,v}]$, a $D \times H$-matrix $Q = [q_{d,h}]$, a $D \times O$-matrix $\overline{Q} = [\overline{q}_{d,o}]$, a $V \times U$-matrix $W = [w_{v,h}]$ and a $H \times O$-matrix $\overline{W} = [\overline{w}_{h,o}]$. Then, (3) can be rewritten as the following matrix manner:

$$\hat{Q} = \min(X, 1), \ Q = \min(\hat{Q}W, 1), \ \overline{Q} = \min(Q\overline{W}, 1), \tag{4}$$

subject to the RNN constraints $W \geq 0, \overline{W} \geq 0, \sum_{h=1}^{H} w_{v,h} \leq 1$ and $\sum_{o=1}^{O} \overline{w}_{h,o} \leq 1$. The problem for the autoecoder to learn the dataset X can be described as

$$\arg\min_{W,\overline{W}} ||X - \overline{Q}||^2, \ \text{s.t.} \ W \geq 0, \overline{W} \geq 0, \sum_{h=1}^{H} w_{v,h} \leq 1, \sum_{o=1}^{O} \overline{w}_{h,o} \leq 1. \tag{5}$$

We use the following update rules to solve this problem, which are simplified from Liu's work [33]:

$$w_{v,h} \leftarrow w_{v,h} \frac{(X^{\mathrm{T}}X\overline{W}^{\mathrm{T}})_{v,h}}{(X^{\mathrm{T}}XW\overline{W}\overline{W}^{\mathrm{T}})_{v,h}}, \tag{6}$$

$$\overline{w}_{h,o} \leftarrow \overline{w}_{h,o} \frac{(W^{\mathrm{T}}X^{\mathrm{T}}X)_{h,o}}{(W^{\mathrm{T}}X^{\mathrm{T}}XW\overline{W})_{h,o}}, \tag{7}$$

where the symbol $(\cdot)_{v,h}$ denotes the element in the vth row and hth column of a matrix. Note that, to avoid the division-by-zero problem, zero elements in the denominators of (6) and (7) are replaced with tiny positive values, (e.g., "eps" in MATLAB). After each update, adjustments need to be made such that W and $\overline{W}$ satisfy the RNN constraints. The procedure to train the shallow LRNN autoencoder (4) is given in Algorithm 1, where the operation $\max(W)$ produces the maximal element in W, the operations of $w_{v,h} \leftarrow w_{v,h}/\sum_{h=1}^{H} w_{v,h}$ and $\overline{w}_{h,o} \leftarrow \overline{w}_{h,o}/\sum_{o=1}^{O} \overline{w}_{h,o}$ guarantee that the weights satisfy the RNN constraints, and the operations $W \leftarrow W/\max(\bar{X}W)$ and $\overline{W} \leftarrow \overline{W}/\max(H\overline{W})$ normalize the weights to reduce the number of neurons that are saturated.

Algorithm 1 Procedure for training a shallow nonnegatvie LRNN autoencder (4)

Randomly initialize W and $\overline{W}$ that satisfy RNN constraints
while terminal condition is not satisfied **do**
    for each minibatch $\bar{X}$ **do**
        update W with (6)
        for $v = 1, \cdots, V$ **do**
            if $\sum_{h=1}^{H} w_{v,h} > 1$
                $w_{v,h} \leftarrow w_{v,h}/\sum_{h=1}^{H} w_{v,h}$, for $h = 1, \cdots, H$
        $W \leftarrow W/\max(\bar{X}W)$
        update $\overline{W}$ with (7)
        for $h = 1, \cdots, H$ **do**
            if $\sum_{o=1}^{O} \overline{w}_{h,o} > 1$
                $\overline{w}_{h,o} \leftarrow \overline{w}_{h,o}/\sum_{o=1}^{O} \overline{w}_{h,o}$, for $o = 1, \cdots, O$
        $H = \min(\bar{X}W, 1)$
        $\overline{W} \leftarrow \overline{W}/\max(H\overline{W})$

---

4 Multi-layer non-negative LRNN autoencoder

We stack multi LRNNs to build a multi-layer non-negative LRNN autoencoder. Suppose the multi-layer autoencoder has a visual layer, M encoding layers and M decoding layer ($M \geq 2$), and they are connected in series with excitatory weights W_m and $\overline{W}$ with $m = 1, \cdots, M$. We import a dataset X into the visual layer of the autoencoder. Let H_m and O_m denote the numbers of neurons in the mth encoding layer and decoding layer, respectively. For the autoencoder, $V = O_M$, $H_m = O_{M-m}$ with $m = 1, \cdots, M - 1$.

Let $\hat{Q}$ denote the state of the visual layer, Q_m denote the state of the mth encoding layer and $\overline{Q}_m$ denote the state of the mth decoding layer. Then, the multi-layer LRNN autoencoder is described by

$$\begin{cases} \hat{Q} = \min(X, 1), \ Q_1 = \min(\hat{Q}W_1, 1), \ Q_m = \min(Q_{m-1}W_m, 1), \\ \overline{Q}_1 = \min(Q_M\overline{W}_1, 1), \ \overline{Q}_m = \min(\overline{Q}_{m-1}\overline{W}_m, 1), \end{cases} \tag{8}$$

with $m = 2, \cdots, M$. The RNN constraints for (8) are $W_m \geq 0$, $\overline{W}_m \geq 0$ and the summation of each row in W_m and $\overline{W}_m$ is not larger than 1, where $m = 1, \cdots, M$. The problem for the multi-layer LRNN autoencoder (8) to learn dataset X can be described as

$$\arg \min_{W_m, \overline{W}_m} ||X - \overline{Q}_M||^2, \tag{9}$$

subject to the RNN constraints, where $m = 1, \cdots, M$. The procedure to train the multi-layer non-negative LRNN autoencder (8) is given in Algorithm 2.

To avoid loading the whole dataset into the computer memory, we could also use Algorithm 3 to train the autoencoder, where the update rules could be

$$W_1 \leftarrow W_1 \odot \frac{\hat{Q}^{\mathrm{T}}\hat{Q}\overline{W}_M^{\mathrm{T}}}{\hat{Q}^{\mathrm{T}}\hat{Q}W_1\overline{W}_M\overline{W}_M^{\mathrm{T}}}, \ W_m \leftarrow W_m \odot \frac{Q_{m-1}^{\mathrm{T}}Q_{m-1}\overline{W}_{M-m+1}^{\mathrm{T}}}{Q_{m-1}^{\mathrm{T}}Q_{m-1}W_m\overline{W}_{M-m+1}\overline{W}_{M-m+1}^{\mathrm{T}}}, \tag{10}$$

$$\overline{W}_M \leftarrow \overline{W}_M \odot \frac{W_1^{\mathrm{T}}\hat{Q}^{\mathrm{T}}\hat{Q}}{W_1^{\mathrm{T}}\hat{Q}^{\mathrm{T}}\hat{Q}W_1\overline{W}_M}, \ \overline{W}_{M-m+1} \leftarrow \overline{W}_{M-m+1} \odot \frac{W_m^{\mathrm{T}}Q_{m-1}^{\mathrm{T}}Q_{m-1}}{W_m^{\mathrm{T}}Q_{m-1}^{\mathrm{T}}Q_{m-1}W_m\overline{W}_{M-m+1}}, \tag{11}$$

with $m = 2, \cdots, M$ and the operation $\odot$ denoting element-wise product of two matrices. To avoid the division-by-zero problem, zero elements in denominators of (10) and (11) are replaced with tiny positive values. The operations of adjusting the weights to satisfy the RNN constraints and normalizing the weights are the same as those in Algorithm 1.

Algorithm 2 Proceduce for training a multi-layer LRNN-based non-negatvie autoencder (8)

$X_1 = X$
for $m = 1, \cdots, M$ **do**
    Train W_m and $\overline{W}_{M-m+1}$ with Algorithm 1 that takes X_m as input dataset
    if $m \neq M$ **do**
        $X_{m+1} = \min(X_m W_m, 1)$

Algorithm 3 Proceduce for training a multi-layer LRNN-based non-negatvie autoencder (8) (mini-batch manner)

Randomly initialize W_m and $\overline{W}_m$ that satisfy RNN constraints (with $m = 1, \cdots, M$)
while terminal condition is not satisfied do
    for each minibatch $\bar{X}$ **do**
        for $m = 1, \cdots, M$ **do**
            update W_m with (10)
            adjust W_m to satisfy RNN constraints
            normalize W_m subject to $\bar{X}$
            update $\overline{W}_m$ with (11)
            adjust $\overline{W}_m$ to satisfy RNN constraints
            normalize $\overline{W}_m$ subject to $\bar{X}$

---

5 Numerical Experiments

5.1 Datasets

MNIST: The MNIST dataset of handwritten digits [29] contains 60,000 and 10,000 images in the training and test dataset. The number of input attributes is 784 (28×28 images), which are in $[0, 1]$.

Yale face: This database (`http://vision.ucsd.edu/content/yale-face-database`) contains 165 gray scale images of 15 individuals. Here we use the pre-processed dataset from [30], where each image is resized as 32×32 (1024 pixels).

CIFAR-10: The CIFAR-10 dataset consists of 60,000 32×32 colour images [31]. Each image has 3072 attributes. It contains 50,000 and 10,000 images in the training and test dataset.

UCI real-world datasets: In addition to image datasets, we also conduct numerical experiments on different real-world datasets in different areas from the UCI machine learning repository [32]. The names, attribute numbers and instance numbers of these datasets are listed in Table 1.

5.2 Convergence and reconstruction performance

Results of MNIST: Let us first test the convergence and reconstruction performance of the shallow non-negative LRNN autoencoder. We use structures of $784 \rightarrow 100$ (for simplicity, we use the encoding part to represent an autoencoder) and $784 \rightarrow 50$ and the MNIST dataset for experiments. The whole training dataset of 60,000 images is used for training. Figure 2(a) shows the curves of training error (mean square error) versus the number of iterations, where, in each iteration, a minibatch of size 100 is handled. Then, we use a multi-layer non-negative LRNN autoencoder with structure $784 \rightarrow 1000 \rightarrow 500 \rightarrow 250 \rightarrow 50$, and the corresponding curve of training error versus iterations is also given in Figure 2(a). It can be seen from Figure 2(a) that reconstruction errors using the LRNN autoencoders equipped with the developed algorithms converge well for different structures. In addition, the lowest errors using the shallow and multi–layer autoencoders are respectively 0.0204 and 0.0190. The results show that, for the same encoding dimension, the performances of the shallow and multi-layer structures are similar for this dataset.

Table 1: Features of different UCI real-world datasets from different areas

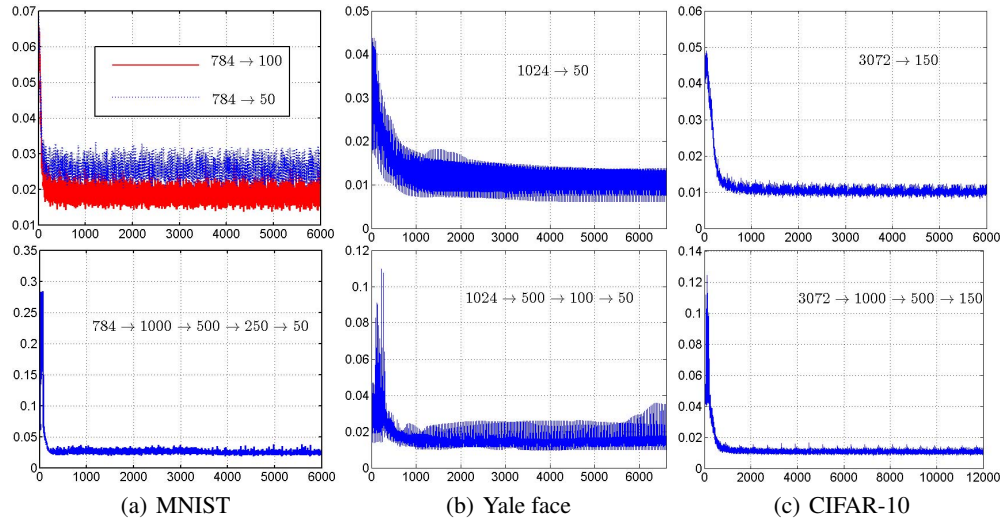| Dataset	Attr. No.	Inst. No.
Iris	4	150
Teaching Assistant Evaluation (TAE)	5	151
Liver Disorders (LD)	5	345
Seeds	7	210
Pima Indians Diabetes (PID)	8	768
Breast Cancer Wisconsin (BC) [34–36]	9	699
Glass	9	214
Wine	13	178
Zoo	16	100
Parkinsons [37]	22	195
Wall-Following Robot Navigation (WFRN) [38]	24	5456
Ionosphere [39]	34	351
Soybean Large (SL)	35	186
First-Order Theorem Proving (FOTP) [40]	51	6118
Sonar [41]	60	208
Cardiac Arrhythmia (CA) [42]	279	452

(a) MNIST (b) Yale face (c) CIFAR-10

Figure 2: Reconstruction error (Y-axis) versus iteration number (X-axis) of shallow and multi-layer LRNN autoencoders for the MNIST, Yale face and CIFAR-10 datasets.

Results of Yale face: Attribute values are normalized into $[0, 1]$ (by dividing by 255). The structures for the shallow and multi-layer LRNN autoencoders are respectively $1024 \rightarrow 50$ and $1024 \rightarrow 500 \rightarrow 100 \rightarrow 50$. The size of a minibatch is 5. Curves of reconstruction errors versus iterations are given in Figure 2(b). For this dataset, the shallow autoencoder seems more stable than the multi-layer one.

Results of CIFAR-10: Attribute values of the dataset are also divided by 255 for normalization in range $[0, 1]$. The structures used are $3072 \rightarrow 150$ and $3072 \rightarrow 1000 \rightarrow 500 \rightarrow 150$. Both the training and testing dataset (total 60,000 images) are used for training the autoencoders. The size of minibatch is chosen as 100. The results are given in Figure 2(c). We can see that reconstruction errors for both structures converge as the number of iterations increases. In addition, the lowest reconstruction errors in using the shallow and multi-layer autoencoders are the same (0.0082). These results together with those with the MNIST and Yale face datasets (Figures 2(a) to 2(c)) verify the good convergence and reconstruction performance of both the shallow and multi-layer LRNN autoencoders for handling image datsets.

Results of UCI real-world datasets: Let N denote the attribute number in a dataset. The structures of the LRNN autoencoders used are $N \rightarrow \text{round}(N/2)$, where the operation round$(\cdot)$ produces
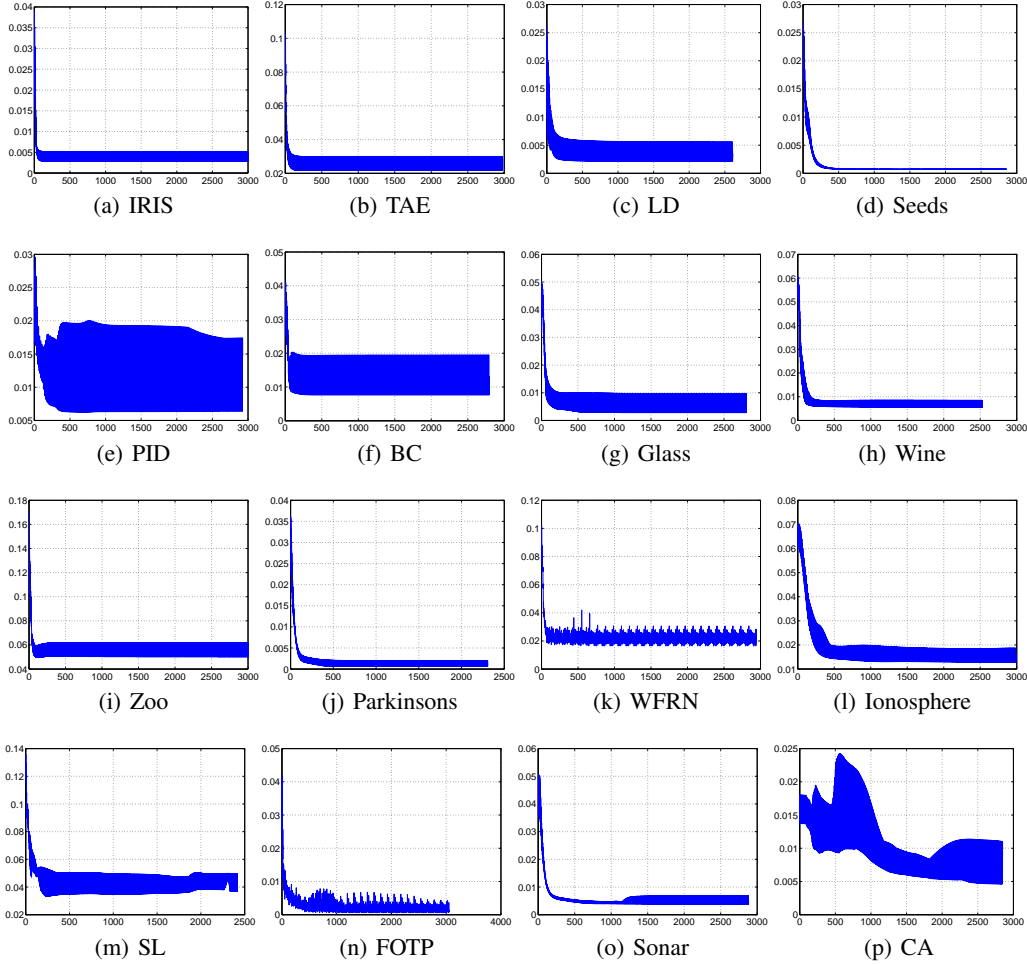
Figure 3: Reconstruction error (Y-axis) versus iteration number (X-axis) of nonnegative LRNN autoencoders for UCI real-world datasets.

the nearest integer number of the element. The attribute values are linear normalized in range $[0, 1]$. The size of mini-batches is set as 50 for all datasets. Curves of reconstruction errors versus iterations are given in Figure 3. We see that the reconstruction errors generally decrease as the number of iterations increases. These results also demonstrate the efficacy of the nonnegative LRNN autoencoders equipped with the training algorithms.

6   Simulating the spiking random neural network

The advantage of a spiking model, such as the LRNN autoencoder, lays on its highly-distributed nature. In this section, rather than numerical calculation, we simulate the stochastic spiking behaviors of the LRNN autoencoder. The simulation in this section is based on the numerical experiment of Subsection 5.2. Specifically, in Subsection 5.2, we construct a LRNN autoencoder of structure $784 \rightarrow 100$ (with appropriate weights found), which has three layers: the visual layer (784 neurons), hidden layer (100 neurons) and output layer (784 neurons). First, an image with $28 \times 28 = 784$ attributes is taken from the MNIST dataset. Each visual neuron receives excitatory spikes from outside the network in a Poisson stream with the rate being the corresponding attribute value in the image. When activated, the visual neurons fire excitatory spikes to the hidden neurons according to the Poisson process with rate 1 (meaning $w_{v,h} = p_{v,h}^+$). When the vth visual neuron fires to the hidden layer, the spike goes to the hth hidden neuron with probability $p_{v,h}^+$ or it goes outside the network with probability $1 - \sum_{h=1}^H p_{v,h}^+$. The hidden neurons fire excitatory spikes to the output
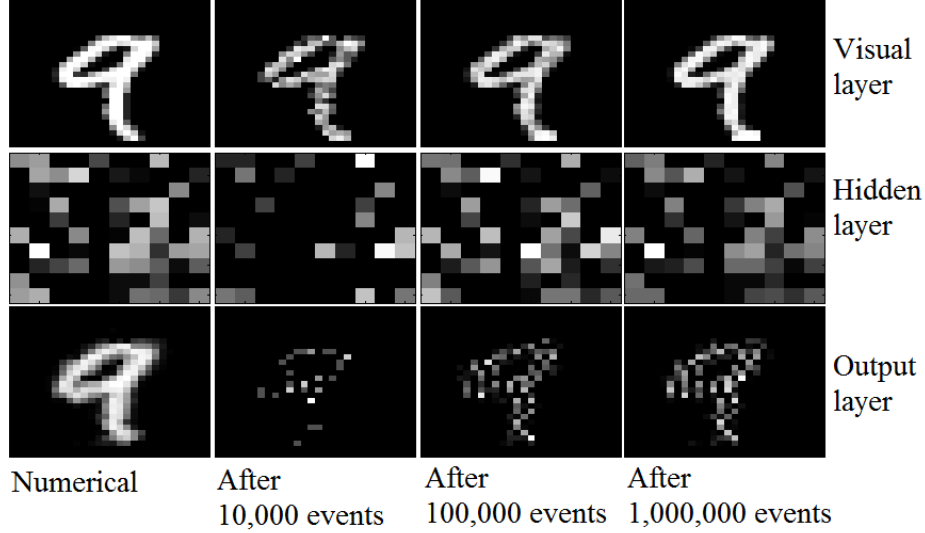
Figure 4: Comparisons between numerical and spiking–behavior simulation results of difference layers in a LRNN autoencoder.

layer in a similar manner subjecting to $\overline{w}_{h,o}$. The firing rate of output neurons is 1 and the spikes go outside the network with probability 1.

In the simulation, we call it an event whenever a spike gets in from outside the network or a neuron fires. During the simulation, we observe the potential (the level of activation) of each neuron once every 1,000 events. Let $k_{i,b}$ represent the bth observation of the ith neuron. We estimate the average potential of the ith neuron, denoted by $\bar{k}_i$, simply by averaging observations, i.e., $\bar{k}_i \approx (\sum_{b=1}^{B} k_{i,b})/B$. Let q_i denote the probability that the ith neuron is activated. The relation between q_i and $\bar{k}_i$ is known as $\bar{k}_i = q_i/(1 - q_i)$. Then, the value of q_i can be estimated during the simulation as:

$$q_i = \frac{\bar{k}_i}{1 + \bar{k}_i} \approx \frac{(\sum_{b=1}^{B} k_{i,b})/B}{1 + (\sum_{b=1}^{B} k_{i,b})/B}. \tag{12}$$

In Figure 4, we visualize the estimated values of q_i for all neurons in different layers after 10,000, 100,000 and 1,000,000 events during the simulation. For comparison, numerical results from Subsection 5.2 are also given in Figure 4. At the beginning, simulation results of only the visual layer are close to its numerical results. As time evolves, the simulation results of the hidden and output layers and their corresponding numerical results become more and more similar. These results demonstrate that the LRNN autoencoders have the potential to be implemented in a highly distributed and parallel manner.

7   Conclusions

New nonnegative autoencoders (the shallow and multi-layer LRNN autoencoders) have been proposed based on the spiking RNN model, which adopt the feed-forword multi-layer network architecture in the deep-learning area. To comply the RNN constraints of nonnegativity and that the sum of probabilities is no larger than 1, learning algorithms have been developed by adapting weight update rules from the NMF area. Numerical results based on typical image datasets including the MNIST, Yale face and CIFAR-10 datesets and 16 real-world datasets from different areas have well verified the robust convergence and reconstruction performance of the LRNN autoencoder. In addition to numerical experiments, we have conducted simulations of the autoencoder where the stochastic spiking behaviors are simulated. Simulation results conform well with the corresponding numerical results. This demonstrates that the LRNN autoencoder can be implemented in a highly distributed and parallel manner.

References

[1] E. Gelenbe, "Random neural networks with negative and positive signals and product form solution," *Neural computation*, vol. 1, no. 4, pp. 502–510, 1989.

[2] ——, "Stability of the random neural network model," *Neural computation*, vol. 2, no. 2, pp. 239–247, 1990.

[3] ——, "Learning in the recurrent random neural network," *Neural Computation*, vol. 5, pp. 154–164, 1993.

[4] E. Gelenbe, V. Koubi, and F. Pekergin, "Dynamical random neural network approach to the traveling salesman problem," in *Proceedings IEEE Symp. Systems, Man and Cybernetics*. IEEE, 1993, p. 630–635.

[5] C. E. Cramer and E. Gelenbe, "Video quality and traffic qos in learning-based subsampled and receiver-interpolated video sequences," *Selected Areas in Communications, IEEE Journal on*, vol. 18, no. 2, pp. 150–167, 2000.

[6] E. Gelenbe and K. F. Hussain, "Learning in the multiple class random neural network," *Neural Networks, IEEE Transactions on*, vol. 13, no. 6, pp. 1257–1267, 2002.

[7] E. Gelenbe, "Steps toward self-aware networks," *Communications of the ACM*, vol. 52, no. 7, pp. 66–75, 2009.

[8] E. Gelenbe and F.-J. Wu, "Large scale simulation for human evacuation and rescue," *Computers & Mathematics with Applications*, vol. 64, no. 12, pp. 3869–3880, 2012.

[9] G. Rubino and M. Varela, "A new approach for the prediction of end-to-end performance of multimedia streams," in *Quantitative Evaluation of Systems, 2004. QEST 2004. Proceedings. First International Conference on the*. IEEE, 2004, pp. 110–119.

[10] S. Mohamed and G. Rubino, "A study of real-time packet video quality using random neural networks," *IEEE Transactions on Circuits and Systems for Video Technology*, vol. 12, no. 12, pp. 1071–1083, 2002.

[11] K. Radhakrishnan and H. Larijani, "Evaluating perceived voice quality on packet networks using different random neural network architectures," *Performance Evaluation*, vol. 68, no. 4, pp. 347–360, 2011.

[12] T. Ghalut and H. Larijani, "Non-intrusive method for video quality prediction over lte using random neural networks (rnn)," in *Communication Systems, Networks & Digital Signal Processing (CSNDSP), 2014 9th International Symposium on*. IEEE, 2014, pp. 519–524.

[13] A. Stafylopatis and A. Likas, "Pictorial information retrieval using the random neural network," *IEEE Transactions on Software Engineering*, vol. 18, no. 7, pp. 590–600, 1992.

[14] H. Larijani and K. Radhakrishnan, "Voice quality in voip networks based on random neural networks," in *Networks (ICN), 2010 Ninth International Conference on*. IEEE, 2010, pp. 89–92.

[15] M. Martínez, A. Morón, F. Robledo, P. Rodríguez-Bocca, H. Cancela, and G. Rubino, "A grasp algorithm using rnn for solving dynamics in a p2p live video streaming network," in *Hybrid Intelligent Systems, 2008. HIS'08. Eighth International Conference on*. IEEE, 2008, pp. 447–452.

[16] G. E. Hinton and R. R. Salakhutdinov, "Reducing the dimensionality of data with neural networks," *Science*, vol. 313, no. 5786, pp. 504–507, 2006.

[17] Y. LeCun, Y. Bengio, and G. Hinton, "Deep learning," *Nature*, vol. 521, no. 7553, pp. 436–444, 2015.

[18] X. Glorot and Y. Bengio, "Understanding the difficulty of training deep feedforward neural networks." in *Aistats*, vol. 9, 2010, pp. 249–256.

[19] G. E. Hinton, S. Osindero, and Y.-W. Teh, "A fast learning algorithm for deep belief nets," *Neural computation*, vol. 18, no. 7, pp. 1527–1554, 2006.

[20] X. Glorot, A. Bordes, and Y. Bengio, "Deep sparse rectifier neural networks." in *Aistats*, vol. 15, no. 106, 2011, p. 275.

[21] O. Bousquet and L. Bottou, "The tradeoffs of large scale learning," in *Advances in neural information processing systems*, 2008, pp. 161–168.

[22] D. D. Lee and H. S. Seung, "Learning the parts of objects by non-negative matrix factorization," *Nature*, vol. 401, no. 6755, pp. 788–791, 1999.

[23] X. Liu, S. Yan, and H. Jin, "Projective nonnegative graph embedding," *IEEE Transactions on Image Processing*, vol. 19, no. 5, pp. 1126–1137, 2010.

[24] P. O. Hoyer, "Non-negative sparse coding," in *Neural Networks for Signal Processing, 2002. Proceedings of the 2002 12th IEEE Workshop on*. IEEE, 2002, pp. 557–565.

[25] Y.-X. Wang and Y.-J. Zhang, "Nonnegative matrix factorization: A comprehensive review," *IEEE Transactions on Knowledge and Data Engineering*, vol. 25, no. 6, pp. 1336–1353, 2013.

[26] C. Ding, T. Li, W. Peng, and H. Park, "Orthogonal nonnegative matrix t-factorizations for clustering," in *Proceedings of the 12th ACM SIGKDD international conference on Knowledge discovery and data mining*. ACM, 2006, pp. 126–135.

[27] E. Wachsmuth, M. Oram, and D. Perrett, "Recognition of objects and their component parts: responses of single units in the temporal cortex of the macaque," *Cerebral Cortex*, vol. 4, no. 5, pp. 509–522, 1994.

[28] C. H. Ding, X. He, and H. D. Simon, "On the equivalence of nonnegative matrix factorization and spectral clustering." in *SDM*, vol. 5. SIAM, 2005, pp. 606–610.

[29] Y. LeCun, L. Bottou, Y. Bengio, and P. Haffner, "Gradient-based learning applied to document recognition," *Proceedings of the IEEE*, vol. 86, no. 11, pp. 2278–2324, 1998.

[30] D. Cai, X. He, Y. Hu, J. Han, and T. Huang, "Learning a spatially smooth subspace for face recognition," in *2007 IEEE Conference on Computer Vision and Pattern Recognition*. IEEE, 2007, pp. 1–7.

[31] A. Krizhevsky and G. Hinton, "Learning multiple layers of features from tiny images," 2009.

[32] M. Lichman, "UCI machine learning repository," 2013. [Online]. Available: http://archive.ics.uci.edu/ml

[33] X. Liu, S. Yan, and H. Jin, "Projective nonnegative graph embedding," *Image Processing, IEEE Transactions on*, vol. 19, no. 5, pp. 1126–1137, 2010.

[34] W. H. Wolberg and O. L. Mangasarian, "Multisurface method of pattern separation for medical diagnosis applied to breast cytology." *Proceedings of the national academy of sciences*, vol. 87, no. 23, pp. 9193–9196, 1990.

[35] O. L. Mangasarian, R. Setiono, and W. Wolberg, "Pattern recognition via linear programming: Theory and application to medical diagnosis," *Large-scale numerical optimization*, pp. 22–31, 1990.

[36] K. P. Bennett and O. L. Mangasarian, "Robust linear programming discrimination of two linearly inseparable sets," *Optimization methods and software*, vol. 1, no. 1, pp. 23–34, 1992.

[37] M. A. Little, P. E. McSharry, S. J. Roberts, D. A. Costello, and I. M. Moroz, "Exploiting nonlinear recurrence and fractal scaling properties for voice disorder detection," *BioMedical Engineering OnLine*, vol. 6, no. 1, p. 1, 2007.

[38] A. L. Freire, G. A. Barreto, M. Veloso, and A. T. Varela, "Short-term memory mechanisms in neural network learning of robot navigation tasks: A case study," in *Robotics Symposium (LARS), 2009 6th Latin American*. IEEE, 2009, pp. 1–6.

[39] V. G. Sigillito, S. P. Wing, L. V. Hutton, and K. B. Baker, "Classification of radar returns from the ionosphere using neural networks," *Johns Hopkins APL Technical Digest*, vol. 10, no. 3, pp. 262–266, 1989.

[40] J. P. Bridge, S. B. Holden, and L. C. Paulson, "Machine learning for first-order theorem proving," *Journal of automated reasoning*, vol. 53, no. 2, pp. 141–172, 2014.

[41] R. P. Gorman and T. J. Sejnowski, "Analysis of hidden units in a layered network trained to classify sonar targets," *Neural networks*, vol. 1, no. 1, pp. 75–89, 1988.

[42] H. A. Guvenir, B. Acar, G. Demiroz, and A. Cekin, "A supervised machine learning algorithm for arrhythmia analysis," in *Computers in Cardiology 1997*. IEEE, 1997, pp. 433–436.